Published in final edited form as:

Mol Pharm. 2016 February 1; 13(2): 357–368. doi:10.1021/acs.molpharmaceut.5b00542.

A Comparative Study on the Alterations of Endocytic Pathways in Multiple Lysosomal Storage Disorders

Jeff Rappaport[#1], **Rachel L. Manthe**[#1], **Melani Solomon**[2], **Carmen Garnacho**[3], and **Silvia Muro**[1,2,*]

[1]Fischell Department of Bioengineering, University of Maryland, College Park, MD 20742-4450, USA

[2]Institute for Bioscience and Biotechnology Research, University of Maryland, 5115 Plant Sciences Building, College Park, MD 20742-4450, USA

[3]Department of Normal and Pathological Histology and Cytology, University of Seville School of Medicine, Seville 41009, Spain

[#] These authors contributed equally to this work.

Abstract

Many cellular activities and pharmaceutical interventions involve endocytosis and delivery to lysosomes for processing. Hence, lysosomal processing defects can cause cell and tissue damage, as in lysosomal storage diseases (LSDs) characterized by lysosomal accumulation of undegraded materials. This storage causes endocytic and trafficking alterations, which exacerbate disease and hinder treatment. However, there have been no systematic studies comparing different endocytic routes or LSDs. Here, we used genetic and pharmacological models of four LSDs (type A Niemann-Pick, type C Niemann-Pick, Fabry, and Gaucher diseases) and evaluated the pinocytic and receptor-mediated activity of the clathrin-, caveolae-, and macropinocytic routes. Bulk pinocytosis was diminished in all diseases, suggesting a generic endocytic alteration linked to lysosomal storage. Fluid-phase (dextran) and ligand (transferrin) uptake via the clathrin route were lower for all LSDs. Fluid-phase and ligand (cholera toxin B) uptake via the caveolar route were both affected, but less acutely in Fabry or Gaucher diseases. EGF-induced macropinocytosis was altered in Niemann-Pick cells, not other LSDs. Intracellular trafficking of ligands was also distorted in LSD vs. wild-type cells. The extent of these endocytic alterations paralleled the level of cholesterol storage in disease cell lines. Confirming this, pharmacological induction of cholesterol storage in wild-type cells disrupted endocytosis, and model therapeutics restored uptake in proportion to their efficacy in attenuating storage. This suggests a proportional and reversible relationship between endocytosis and lipid (cholesterol) storage. By analogy, the accumulation of biological material in other diseases, or foreign material from drugs or their carriers, may cause similar deficits, warranting further investigation.

Abstract

[*]Address correspondence to: Silvia Muro, 5115 Plant Sciences Building, College Park, MD 20742-4450. Tel: 1+301-405-4777; Fax: 1+301-314-9075; muro@umd.edu. .

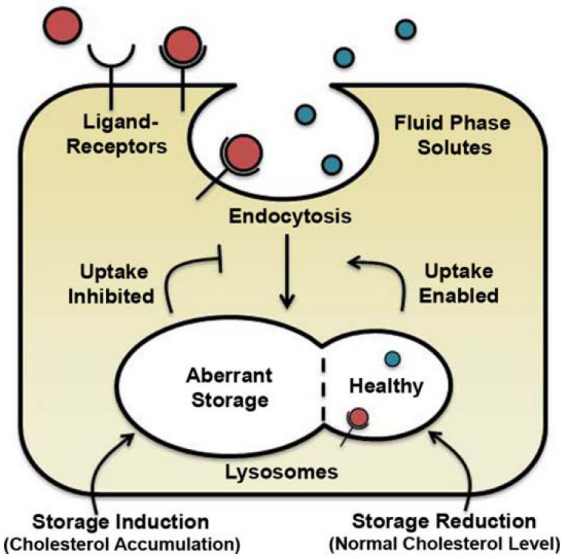

Keywords

Lysosomal storage diseases; endocytosis pathways; enzyme replacement therapy; ICAM-1-targeted nanocarriers; lysosomal storage reduction

Introduction

Through endocytosis, cells internalize plasma membrane components and extracellular materials in membrane-bound vesicles[1]. Subsequent trafficking of internalized cargo to the lysosome (herein referred to as the endo-lysosomal route) and the processing by acidic hydrolases within the lysosomal lumen form the basis of numerous cell functions [1, 2]. These include the use of nutrients and maintenance of metabolic homeostasis, the degradation of apoptotic, autophagic, and pathogenic material, the transduction of cell growth and other regulatory signals, the recycling and modulation of the plasmalemma composition and function, among others [1, 2]. Moreover, lysosomes are the main destination for drugs and/or drug carriers that enter cells via endocytosis [3, 4]. This can be an obstacle to therapy when drugs and their carriers get trapped and degraded in lysosomes, or an advantage when lysosomal cues (enzymes, pH, etc.) are used to control drug release or trigger escape to the cytosol [3-5]. In addition, endo-lysosomal trafficking is required in diseases where the therapeutic target is the lysosome itself [4-6]. Hence, endocytic and lysosomal processes are of great fundamental and translational interest.

Endocytosis occurs via distinct pathways, each having different biological roles and relevance to drug delivery [1, 3, 5]. The most common pathways are those that internalize fluid and dissolved solutes, termed pinocytosis, some of which also concentrate cell-surface receptors with affinity for specific extracellular ligands [1, 3, 5]. Delivery of therapeutic molecules within cells can be designed to follow the fluid phase or actively target these receptors [3, 7, 8]. The most ubiquitous pinocytic pathway is clathrin-mediated endocytosis, which regulates receptors involved in cell signaling and uptake of ligands like low density

lipoprotein, transferrin (Tf), etc. [9]. Therapeutic strategies targeting receptor-mediated uptake via clathrin-coated vesicles have been widely explored [8, 10]. Another common pinocytic pathway is caveolae-mediated endocytosis, characterized by caveolin-1-rich vesicles that form in lipid raft domains of the plasma membrane [11]. Therapeutics bearing albumin, cholera toxin B (CTB), or antibodies to aminopeptidase P, PV1, GM1, and other caveolae components have been shown to internalize within caveolar vesicles [8, 10, 12]. Given the small size of endocytic vesicles resulting from these two pathways, commonly within 50-150 nm in diameter, pinocytosis via the clathrin- and caveolae-mediated routes are also referred to as micropinocytosis [3, 10]. In contrast, in the third of the classical pinocytic mechanisms, macropinocytosis, vesicles do not concentrate specific receptors, but instead internalize large volumes of fluid (vesicle diameter > 500 nm) to promote cell growth, sample antigens, etc. [13]. Although especially active in macrophages and dendritic cells, this pathway can be transiently induced by growth factors in other cell types, therefore playing a broad biological and translational role [7, 13]. In addition to these three classical pinocytic pathways, less common routes of pinocytic uptake have been observed in association with certain cell-surface receptors (e.g. interleukin-2, intercellular adhesion molecule-1 (ICAM-1), etc.) [14], which are far less understood, but appear amenable to intracellular drug delivery [8, 15].

Importantly, defects in endocytosis, trafficking, or lysosomal processing can cause and/or exacerbate disease. Numerous cancers, autoimmune diseases, and neurodegenerative disorders (e.g. Huntington's, Alzheimer's, and Parkinson's) have been linked to storage of undigested material in autophagic and lysosomal compartments, where the affected tissues exhibit inflammation, nutrient deprivation, apoptotic signaling, and other problems [4]. Lysosomal storage diseases (LSDs) offer a clinical example and research model of these effects. LSDs include about 50 different disorders, which arise from inherited mutations that render hydrolases and other lysosomal components ineffective or absent, disrupting lysosomal functions [16]. Non-degraded substrates accumulate, affecting not only the metabolic flux, but also causing intracellular "traffic jams" that interfere with fusion of pre-lysosomal compartments (e.g. autophagosomes and endosomes), biosynthetic and secretory activity, cytoskeletal restructuring, compartment transport, and other homeostatic activities [16-20]. Lysosomal dysfunction often results in developmental abnormalities, peripheral organ damage, progressive central nervous system degeneration, and premature mortality [16].

Interference with the endo-lysosomal route may also impair drug delivery and success of therapeutic approaches [4]. LSDs offer an example. The most common therapy for LSD patients is intravenous administration of recombinant enzymes to replace those absent in the disease [6, 21]. Glycosylation motifs on these enzymes bind to cell-surface mannose-6-phosphate receptors, or the enzymes can be modified to target other clathrin-associated receptors [6, 21]. In principle, cells then take up the enzymes via clathrin-mediated endocytosis and deliver them to lysosomes to clear stored substrates [6, 21]. However, several groups have observed alterations in the behavior of endocytic receptors and pathways in LSDs [22-27]. These alterations impact intracellular delivery and effects of therapeutic enzymes [28-31], such as the case of acid sphingomyelinase (ASM) required for treatment of type A Niemann-Pick disease (NPD) [28-30].

Despite these observations, there are few systematic and comparative investigations examining the implications of aberrant lysosomal storage on endocytic uptake and endocytic-dependent therapies. Our recent studies revealed alterations in fluid-phase and receptor-mediated uptake via clathrin-, caveolae-, and macropinocytic-mediated pathways in model NPD cells [29, 30]. Whether such alterations occur in other LSDs is unknown; therefore, here we have examined examples characterized by different genetic defects and primary storage materials: type C Niemann-Pick disease (NPC), characterized by a deficiency of the lysosomal transporter protein NPC1 and primary storage of cholesterol [32]; Fabry disease, characterized by a deficiency of lysosomal α-galactosidase A and primary storage of globotriaosylceramide [33]; and Gaucher disease, characterized by a deficiency of glucocerebrosidase and primary storage of glucocerebroside [34]. We have used genetic and pharmacological models to evaluate the relationship between lysosomal storage, endocytic and trafficking abnormalities, lipid levels, and the therapeutic potential of delivery strategies aimed to normalize endocytic activity and lipid levels. In all these examples, we have found a relationship between aberrant lysosomal storage and altered endocytic activity, which in turn impacts uptake and therapeutic effect. We discuss the implications for cellular health and drug delivery.

Methods

Antibodies and Reagents

Alexa Fluor 488-, Alexa Fluor 594-, and fluorescein-labeled Tf or CTB, fluorescent secondary antibodies, Texas Red dextran (10,000 MW), and BODIPY-FL-C_{12}-sphingomyelin were from Invitrogen Molecular Probes (Carlsbad, CA). Antibodies to Tf and CTB were from Calbiochem (La Jolla, CA), and those against EEA-1 or LAMP-1 were from Calbiochem (La Jolla, CA) or Santa Cruz Biotechnology (Dallas, TX), respectively. Antibody to ganglioside GM1 was obtained from the Developmental Studies Hybridoma Bank, created by the NICHD of the NIH and maintained by The University of Iowa, Department of Biology (Iowa City, IA). Polystyrene beads (100 nm diameter) were from Polysciences (Warrington, PA). Mouse monoclonal antibody against human ICAM-1 (anti-ICAM; clone R6.5) was from the American Type Culture Collection (Manassas, VA). Recombinant human ASM [35] was kindly provided by Dr. Edward Schuchman (Dept. of Genetics and Genomic Sciences, Mount Sinai School of Medicine, New York, NY). Unless otherwise noted, all other reagents were from Sigma Aldrich (St. Louis, MO).

Cell Cultures

Primary skin fibroblasts obtained from wild-type and NPD patients (homozygous for the R496L mutation) were kindly provided by Dr. Edward Schuchman. Primary skin fibroblasts from patients of NPC, Gaucher, and Fabry diseases were from the NIGMS Human Genetic Cell Repository of the Coriell Institute (Camden, NJ) and were homozygous for C39F, homozygous for L444P, and hemizygous for W162X mutations, respectively. Cells within 10 passages were seeded on glass coverslips and incubated at 37°C, 5% CO_2, and 95% relative humidity in Dulbecco's Modified Eagle Medium (Gibco BRL, Grand Island, NY) supplemented with 10% fetal bovine serum, 2 mM glutamine, 100 U/mL penicillin, and 100 μg/mL streptomycin. Where indicated, ICAM-1 expression was stimulated as in

inflammatory conditions pertaining to LSDs [15, 36], by incubating cells with 10 ng/mL tumor necrosis factor α (TNFα) overnight prior to assays.

Validation of Uptake via Selected Pathways

Similar to previous works [37], we validated the endocytic models used in this study. For this purpose, wild-type fibroblasts were incubated for 30 min at 37°C with 1 mg/mL Texas Red dextran (10,000 MW), a fluid-phase marker for endocytosis, in the presence of 200 μg/mL Tf or 33.3 μg/mL CTB, ligands of clathrin- or caveolae-mediated endocytosis, respectively, conjugated to green fluorescein or Alexa Fluor 488. Cells were washed, fixed with cold 2% paraformaldehyde, and imaged by fluorescence microscopy. Alternatively, cells incubated with Texas Red dextran alone were washed, fixed, and permeabilized for 5 min with 0.2% Triton X-100, followed by immunostaining of ganglioside GM1 detected using a green Alexa Fluor 488-labeled secondary antibody.

Samples were examined using an Eclipse TE2000-U microscope, 60x PlanApo objectives, and filters optimized for Texas Red and FITC fluorescence (Nikon, Melville, NY). Separate color channels were imaged with an Orca-ICCD camera (Hamamatsu, Bridgewater, NJ), merged, and analyzed with ImagePro 3.0 software (Media Cybernetics, Silver Spring, MD). In merged-channel images, uptake of red dextran within green Tf-, CTB-, or ganglioside GM1-containing vesicles was visualized as colocalization of these colors (yellow), indicating co-uptake via clathrin- or caveolae-mediated endocytosis. This was quantified using a customized algorithm that detects fluorescent pixels and endosomal-sized vesicles surpassing background threshold fluorescence [29, 30]. The percentage of colocalization was calculated for each cell using the total fluorescence area occupied by each label and total number of endosome-size vesicles occupied by each label, whereby the cell borders were obtained by phase-contrast microscopy [29, 30].

In addition, uptake of Texas Red dextran via macropinocytosis was induced by co-incubation for 30 min at 37°C with 100 ng/mL epidermal growth factor (EGF), which stimulates the formation of membrane ruffles [13]. This was tested in the absence vs. presence of 3 mM amiloride, which is known to inhibit macropinocytosis. In each cell, the total number of endocytic vesicles occupied by dextran was quantified as described above, and uptake was compared between control and amiloride conditions.

Further validation consisted of incubating wild-type fibroblasts for 30 min or 1 h at 37°C with red Alexa Fluor 594-conjugated Tf (200 μg/mL) or CTB (33.3 μg/mL), respectively. This was done in the absence (control condition) vs. presence of 50 μM monodansylcadaverine (MDC; to inhibit clathrin endocytosis), 1 μg/mL filipin (to inhibit caveolar endocytosis), or 3 mM amiloride (to inhibit macropinocytosis induced by EGF). Cells were washed, fixed, and surface-located (non-internalized) Tf or CTB were immunostained using antibodies conjugated to green FITC. Samples were analyzed by fluorescence microscopy using the customized algorithm described above [29, 30], which required Tf or CTB to be pseudocolored in green, while the additional cell-surface stains were pseudocolored in red. Therefore, in merged-channel images, surface Tf or CTB appear yellow vs. internalized counterparts that appear green [29, 30]. The percentage of internalized

green fluorescent pixels over the total cell-associated fluorescence per cell was quantified, whereby the cell borders were obtained by phase-contrast microscopy [29, 30].

Fluid-Phase Uptake in Wild-Type vs. LSD Cells

To compare bulk fluid-phase pinocytosis as well as the contribution of individual pathways in wild-type vs. diseased fibroblasts, cell were incubated for 1 h at 37°C with 1 mg/mL Texas Red dextran in control cell medium or medium containing 50 μM MDC or 1 μg/mL filipin. Alternatively, macropinocytosis was evaluated by incubating cells for 1 h at 37°C with 1 mg/mL Texas Red dextran in medium containing 100 ng/mL EGF. Cell samples were washed, fixed, and the number of fluorescent dextran-filled compartments per cell (cell borders were observed by phase-contrast) was quantified by fluorescence microscopy, as described [29, 30].

Ligand Uptake in Wild-Type vs. LSD Cells

To measure receptor-mediated uptake by either clathrin- or caveolae-mediated endocytosis, wild-type vs. diseased fibroblasts were incubated for 1 h at 37°C in cell medium containing 200 μg/mL Tf or 33.3 μg/mL CTB, respectively, both conjugated to red Alexa Fluor 594 [29, 30]. Cells were washed, fixed, and cell surface-located ligands were immunostained using green FITC-conjugated antibodies. As described above, samples were analyzed by fluorescence microscopy, whereby surface Tf or CTB appear yellow vs. internalized counterparts that appear green [29, 30]. The percentage of internalized green fluorescent pixels over the total cell-associated fluorescence, and the number of green fluorescent vesicles per cell were quantified, where the cell borders were obtained by phase-contrast microscopy [29, 30]. LSD cells were compared to wild-type cells, and control conditions were compared to inhibitor conditions, as described.

Scanning Electron Microscopy Visualization

Similar to our previous SEM examination of clathrin-coated pits in wild-type vs. NPD cells [30], we imaged cells for the presence of caveoli. We defined cell-surface caveoli as invaginations on the plasmalemma with a size ≤ 50 nm in diameter and void of an electron-light halo surrounding the opening of the invagination (this halo is characteristic of clathrin-coated pits) [30]. Semiquantitative analysis was performed to analyze the number of invaginations per cell-surface area.

Intracellular Trafficking of Ligands in Wild-Type vs. LSD Cells

Cells were incubated for 30 min at 37°C with 200 μg/mL Tf or 33.3 μg/mL CTB, both conjugated to red Alexa Fluor 594. Samples were then washed, fixed, and permeabilized as described above. Early endosomal compartments were then labeled using anti-EEA-1 followed by a secondary antibody conjugated to green Alexa Fluor 488. Alternatively, lysosomes were marked using green Alexa Fluor 488-conjugated anti-LAMP-1. Cells were visualized by fluorescence microscopy, whereby colocalization of red-labeled ligands (Tf or CTB) with green-labeled compartment markers, which appear yellow in color-merged images, was analyzed using the algorithms described above. This colocalization was

expressed as a percentage of the total ligands present in cells, and the number of EEA-1 or LAMP-1 positive vesicles were additionally quantified.

Imaging of Lipid Storage in Wild-Type vs. LSD Cells

To track sphingomyelin levels, wild-type vs. diseased fibroblasts were incubated overnight with fluorescent BODIPY-FL-C_{12}-sphingomyelin, which fluoresces red (620 nm) at high concentrations and green (530 nm) at physiological concentrations [38], and cells were then fixed. In parallel experiments, in order to track cholesterol levels, cells were fixed and stained with 50 μg/mL filipin, which binds to cholesterol and fluoresces blue. Sphingomyelin or cholesterol staining were quantified by fluorescence microscopy, as previously described [38, 39].

Preparation of ASM-Loaded Nanocarriers Targeted to ICAM-1

Model polymer nanocarriers were prepared by surface adsorption of a 50:50 mass ratio of anti-ICAM and ASM onto 100 nm-diameter polystyrene beads (anti-ICAM/ASM NCs), as described [38]. Carriers were centrifuged at 13,000 g for three minutes to remove unbound molecules, re-suspended in phosphate buffered saline supplemented with 1% bovine serum albumin, and sonicated at low power. This procedure produces carriers that target and deliver active ASM to the lysosome, capable of degrading accumulated substrates [29, 38]. Anti-ICAM or ASM cargo were characterized via conjugation to ^{125}I and quantification of radiolabeled protein with a gamma counter, as reported [38]. The diameter and polydispersity index of the coated particles were 190 ± 7 nm and 0.16 ± 0.02, respectively, measured by dynamic light scattering. Carriers contained 230 ± 24 ASM molecules and 135 ±17 anti-ICAM molecules per particle. This formulation has been shown to exhibit minimal enzyme release by mechanical stress (~10% release), storage (<5% release after three days in saline at 4°C), or physiological-like conditions (~10% release after 5 h in serum at 37°C), with lack of serum protein (albumin) absorption [40, 41]. These are prototype carriers, with coating efficacy, *in vivo* targeting, and intracellular transport comparable to anti-ICAM NCs made of biodegradable poly(lactic-co-glycolic acid) [42, 43], therefore providing a valid model for cell culture assays. In addition, the specificity of anti-ICAM NCs (vs. control IgG NCs) in terms of targeting, endocytic uptake, and lysosomal delivery has been extensively demonstrated in both cell cultures and mouse models [29, 37, 39-43].

Modulation of Lipid Storage Levels

To determine the role of lipid storage on endocytic uptake, TNFα-stimulated wild-type and NPD fibroblasts were treated to modulate lipid levels as follows. To induce lipid storage independently of genotype, wild-type cells were incubated for 48 hours at 37°C with 50 μM imipramine, which cleaves endogenous ASM and renders it inactive [44]. Contrarily, to reduce lipid storage, NPD fibroblasts were incubated for 1 h at 37°C with 500 μM methyl-β -cyclodextrin (a ring-shaped polysaccharide that removes cholesterol from cells [45]), or for 3 h with recombinant ASM (1 h pulse + 2 h chase with ASM-free media). This enzyme was administered either as a naked counterpart (32 nM vs. 320 nM) or coupled onto anti-ICAM NCs (32 nM ASM). After these treatments, cells were washed, and lipid levels and dextran uptake were assessed via fluorescence microscopy, as described above.

Statistics

Fluorescence experiments involved two or three assays and microscopy analysis involved random selection of 8-15 regions located throughout the sample for image acquisition. Each region contained a range of cells (4-10). Cells contained in each image were individually analyzed, where all vesicles contained per cell were included in the analysis (this represents a total between 1,000-3,000 vesicles per condition). For SEM assays, images from two independent samples were analyzed (≥103 invaginations analyzed per condition). Data were calculated as mean ± standard error of the mean (SEM), where statistical significance was determined as $p<0.05$ by Student's t-test, since comparisons were made between two groups.

Results

Reduced Fluid-Phase Uptake in Bulk and via Clathrin or Caveolar Pathways in LSD Fibroblasts

Non-specific pinocytosis serves as the gateway for extracellular fluid and dissolved solutes (including many drugs) to enter the cell. We recently demonstrated that lysosomal storage in NPD impairs bulk pinocytosis [29, 30]. To examine if this is also the case for other LSDs, we compared the uptake of Texas Red dextran, a fluid-phase marker, in fibroblasts from patients of NPC, Gaucher, and Fabry diseases (Fig. 1). Over the course of one hour, all fibroblast types accumulated fewer dextran-filled compartments than wild-type cells, as observed by fluorescence microscopy (Fig. 1a), consistent with our previous findings in NPD cells [29, 30]. Automatic image analysis revealed ~40% fewer dextran-positive vesicles in diseased cells vs. wild-type cells (Fig. 1b), suggesting a similar pinocytic alteration in all of these diseases.

This decrease in dextran uptake may be attributed to alteration in one or a combination of the pathways that contribute to bulk pinocytosis: clathrin-, caveolae-, and macropinocytic-mediated endocytosis [1]. For most cells, clathrin-coated pits and caveoli are the most likely uptake mechanisms, since macropinocytosis is largely restricted to immune cells and cells transiently stimulated by growth factors [13]. In fact, as shown in Fig. 2a, fluorescent dextran internalized by wild-type cells significantly colocalized with ligands that associate with the clathrin route [9] (41-48% colocalization with transferrin; Tf) or the caveolar route [29, 46] (48-53% colocalization with cholera toxin B; CTB). Since a fraction of CTB may enter certain cells via the clathrin pathway [47], we further confirmed dextran uptake via caveoli in wild-type cells by colocalization with a lipid raft domain constituent: the CTB target, ganglioside GM1 (40-55% colocalization; Suppl. Fig. 1).

The contribution of clathrin and caveolar pathways to endocytosis has been shown to differ between different cell types and tissue culture conditions [48-51]. In this particular case, the validation described above indicates that these two routes contributed similarly to dextran uptake in wild-type fibroblasts. This parallels our previous data [29, 30] and was also confirmed here (left bars in Fig. 2b and 2c), showing that dextran uptake was diminished by 43% and 44% in the presence of MDC or filipin, which respectively inhibit the clathrin and caveolar routes. Verifying the specificity of the inhibitors and conditions used, MDC decreased uptake of Tf but not CTB, filipin inhibited uptake of CTB but not Tf, and

amiloride (a macropinocytosis inhibitor) did not affect the uptake of either of these ligands (Suppl. Fig. 2).

With regard to the behavior of LSD cells, as previously observed for NPD cells [30] and confirmed here (Fig. 2b), MDC had no significant effect on dextran uptake: 96%, 102%, 105%, and 91% of control for NPD, NPC, Gaucher, and Fabry cells, respectively (Fig. 2b). This indicates that the clathrin pathway was already diminished in all these cells and MDC had no further effect. As per the caveolar route (Fig. 2c), filipin did not significantly diminish dextran uptake in NPD cells (84% of control conditions), indicating that the pathway is affected in this disease, as described [29]. This was further confirmed by scanning electron microscopy (see Materials and Methods), which showed 52 caveolar-like invaginations per 100 μm^2 of cell-surface area for NPD cells vs. 131 for wild-type fibroblasts, a 60% reduction (Suppl. Fig. 3). Similarly to NPD, filipin did not diminish dextran uptake in NPC cells (81% of control), suggesting that the caveolar route is also affected in this disease (Fig. 2c). This was not the case for Gaucher and Fabry cells, where filipin decreased dextran uptake by 35% and 30% respectively, as in wild-type cells (Fig. 2c).

Reduced Fluid-Phase Uptake via Macropinocytosis in LSD Fibroblasts

Finally, we evaluated the contribution of macropinocytosis to non-specific fluid-phase uptake. Since clathrin- and caveolae-mediated pathways contributed almost the totality of dextran uptake in these fibroblasts (Fig. 2), we induced macropinocytosis by incubating cells with dextran in the presence of EGF. This signaling molecule results in the formation of membrane ruffles on the cell surface in non-immune cells and, hence, induces macropinocytosis [13]. Verifying this premise, amiloride inhibited dextran uptake in wild-type cells (Suppl. Fig. 4), while it did not affect the uptake of Tf or CTB. In turn, MDC or filipin, which inhibited uptake of Tf and CTB, respectively (Suppl. Fig. 2 described above), did not inhibit dextran uptake induced by EGF (data not shown). With this verification in place, we examined the behavior in disease. The number of dextran-filled vesicles internalized by macropinocytosis varied among LSD cells (Fig. 3a): compared to wild-type cells, uptake was diminished by 33% in NPD cells (as previously reported [29]), enhanced by 35% in NPC cells (Fig. 3b), and no significant differences were found for Gaucher and Fabry cells (Fig. 3a and 3b).

Altogether, the findings reported in this and the previous sections suggest that endocytic alterations may be common to many LSDs, yet the activity of individual pathways may vary in each particular disease.

Reduced Endocytosis of Clathrin- and Caveolae-Associated Ligands in LSD Fibroblasts

Given the alterations observed in fluid-phase uptake, both collectively and by individual pathways, we next examined uptake of specific ligands via clathrin- and caveolae-mediated endocytosis. First, we used fluorescent Tf as a model ligand that binds to the Tf receptor, which internalizes via the clathrin pathway [9]. Over the course of one hour, the number of Tf-positive vesicles was visibly lower for all diseased fibroblasts as compared to wild-type cells (Fig. 4a), which is consistent with observations previously reported for NPD cells [30]. Image

quantification revealed that in wild-type fibroblasts, 93% of the total Tf associated with cells was found intracellularly, whereas this parameter ranged from 66% to 72% in diseased fibroblasts (Fig. 4b). Since the internalization percentage reflects the uptake rate, we also compared the absolute level of surface-bound and internalized Tf in these cells. A comparable level of Tf was found bound on the surface of all cell types (from 6-16 fluorescent objects; Fig. 4c). In turn, the difference arose when comparing internalized Tf levels: 17-32 vesicles in diseased cells vs. 136 in wild-type cells (Fig. 4c), suggesting a defect in the internalization mechanism and consistent with the diminished fluid-phase uptake observed.

We also examined the uptake of fluorescent cholera toxin B (CTB), a ligand that binds to ganglioside GM1 on the cell surface and is primarily internalized within caveolae [46], as recently verified in these fibroblasts [29]. In wild-type cells, CTB accumulated in a perinuclear region, consistent with expected Golgi and endoplasmic reticulum localization [52], whereas it appeared to localize in more punctate compartments in diseased cells (Fig. 5a). Quantification of the uptake efficiency (Fig. 5b) showed that the rate of CTB uptake in wild-type cells was 76% of all cell-associated CTB, while this parameter was reduced for NPC (46% uptake), much like previously reported for NPD (49% uptake) [29]. This was not the case for Fabry and Gaucher cells, which showed uptake rates similar to wild-type (70% and 76%, respectively). A comparable level of CTB was bound to the surface of wild-type, NPD, NPC, and Gaucher cells (from 33 to 55 fluorescent objects; Fig. 5c), while less surface-bound material was associated with Fabry cells (24 objects). More significant differences were observed when comparing internalized material: 148 vesicles in wild-type cells vs. 43 and 47 in NPD and NPC, respectively (Fig. 5c). A more mild, yet significant decrease was also observed for Gaucher and Fabry cells (84 and 72 vesicles/cell). Hence, like the clathrin pathway, caveolae-mediated ligand uptake appears to be diminished in LSDs, although a greater variation was observed between diseases.

Intracellular Trafficking of Ligands in LSD Fibroblasts

After identifying these endocytic alterations in LSDs, we next evaluated potential changes in the intracellular trafficking of ligands internalized via clathrin- or caveolae-mediated pathways. For this purpose, we examined the colocalization of Tf or CTB with markers of early endosomes (EEA-1) or lysosomes (LAMP-1). Fluorescence microscopy visualization (Suppl. Fig. 5) and quantification (Fig. 6a) showed an enhanced number of both early endosomes and lysosomes in NPD compared to wild-type cells (149% and 152% of wild-type levels, respectively), which is expected in LSDs [4,16]. Most importantly, a lower fraction of Tf and CTB colocalized with endosomal compartments (67% and 78% of the wild-type level; Fig. 6b and Suppl. Fig. 5a), and this was also the case for colocalization of these ligands with lysosomes (23% and 70% of the wild-type level; Fig. 6c and Suppl. Fig. 5b). Therefore, intracellular trafficking also seems to be altered in LSDs, which may be a consequence of the lower rate of endocytosis.

Lipid Storage Correlates with Endocytic Dysfunction

The fact that altered endocytic patterns are observed for several LSDs despite their different genetic defects, metabolic routes involved, and storage materials suggests a generic link

between lysosomal and endocytic dyfunctions (e.g. sequestration of endocytic machinery, compartment mistrafficking, altered signaling, etc.). Specifically, vesiculation and vesicle trafficking depends on membrane lipid composition, of which cholesterol and other lipid raft constituents, such as sphingomyelin, are key regulatory components [24, 53, 54]. Therefore, we examined the relative levels of cholesterol and sphingomyelin in these LSD cells. Fluorescence microscopy showed that, compared to wild-type fibroblasts, cells from all four diseases accumulated both lipids at higher levels (Fig. 7a): Gaucher and Fabry diseases cells accumulated 2-3-fold more cholesterol and sphingomyelin than wild-type cells, and NPD and NPC fibroblasts accumulated ~4-5 fold more than wild-type (Fig. 7b). These data correlate well with the broader and more severe endocytic alterations observed in NPD and NPC cells, suggesting a relationship between said lipid levels and endocytic activity.

In order to explore this possible relationship, we focused on NPD cells as an example of high lipid accumulation and alterations in all classical endocytic pathways compared to healthy cells. Using this example, we manipulated cholesterol levels and assessed the outcome with regard to bulk fluid-phase endocytosis (using Texas Red dextran), since this represents the additive uptake through all pathways (Fig. 8a). First, wild-type fibroblasts were treated with imipramine, which degrades endogenous ASM, mimicking ASM inactivity characteristic of NPD. This led to increased cholesterol storage up to a level comparable to that of NPD fibroblasts (4.4-fold over untreated healthy cells; 116% of NPD cells) and reduced dextran uptake (45% of untreated wild-type cells; 90% of NPD cells). The reverse was true as well: treatment of NPD fibroblasts with methyl-β-cyclodextrin to remove cholesterol resulted in restoration of cholesterol levels (26% of untreated NPD cells; 97% of wild-type cells) and increased dextran uptake (1.6-fold over untreated NPD cells; 82% of wild-type cells). This demonstrates a link between cholesterol storage and endocytic activity, and suggests that attenuation of cholesterol storage may help normalize the endocytic activity of these cells.

Diminished endocytosis in cholesterol-storing cells represents an important factor for therapeutic design, such as the case of enzyme replacement therapy for LSDs, which depends on endocytic uptake for trafficking to the compartment (the lysosome) in need of said therapeutic activity [4, 21]. We previously showed that deficient clathrin-mediated endocytosis in NPD fibroblasts limited the uptake of therapeutic recombinant ASM from the cell medium, resulting in only a partial attenuation of the enzyme substrate characteristic of this disease, sphingomyelin [30]. This paired well with previous reports that had found reduced uptake via the clathrin-dependent mannose-6-phosphate receptor in ASM deficient cells [28]. In contrast, coupling ASM to nanocarriers targeting intercellular adhesion molecule-1 (ICAM-1), a cell-surface molecule overexpressed in inflammation found in several LSDs [15, 36], which utilizes the clathrin- and caveolae-independent CAM-pathway [30, 37, 38], improved ASM delivery by 10-fold, normalized sphingomyelin storage to wild-type levels, and recovered endocytosis [29, 30]. In addition, targeting, uptake, lysosomal delivery, and intra-lysosomal activity of ASM have been shown to be specific to anti-ICAM NCs vs. control IgG NCs [29, 37, 40-43, 55, 56]. The characterization of these NCs is provided in the Materials and Methods section.

We have shown that these treatments enhance endocytosis and here we demonstrate that this outcome associates with a reduction of cholesterol storage. As shown in Fig. 8b, NPD fibroblasts treated with 32 nM of naked recombinant ASM (low dose) continued to store 3-fold more cholesterol than wild-type cells (86% of untreated NPD cells) and dextran uptake in these cells remained well below wild-type levels (47% of wild-type), comparable to untreated NPD cells (96% of NPD). Increasing the enzyme concentration by 10-fold (320 nM; high dose) restored normal cholesterol levels (101% of wild-type) and partially restored dextran uptake (1.4-fold increase over untreated NPD; 68% of wild-type). Treatment with nanocarrier-loaded ASM both reduced cholesterol levels (65% reduction compared to untreated NPD; 135% of wild-type) and restored fluid-phase uptake (2-fold enhancement compared to untreated NPD; 98% of wild-type) even when using a low enzyme dose (32 nM). Therefore, it appears that endocytic performance in LSDs is linked to lipid levels and strategies able to normalize said levels (methyl-β-cyclodextrin, recombinant ASM, ASM-loaded nanocarriers) have a positive impact on the endocytic activity.

Discussion

Endocytosis followed by lysosomal transport supports numerous cellular functions and is often exploited for intracellular drug delivery [1, 3, 10]. Disruption of lysosomal function can alter endocytic behavior, which may exacerbate disease and impair drug uptake, as is observed in several cancers, autoimmune diseases, and metabolic disorders [4]. Although reports have linked lysosomal dysfunctions to altered endocytosis [19, 20, 22-31, 57], the comparative activity of individual endocytic pathways in cells affected by lysosomal-associated diseases remains unexplored, limiting our ability to optimize therapeutic strategies. LSDs represent adequate models to examine these aspects since they relate to primary lysosomal defects with well-known etiology [4, 18, 19], for which they were used in this study.

As an example, using patient fibroblasts from NPD, an LSD caused by ASM deficiency [58], we recently reported endocytic alterations in the clathrin, caveolar, and macropinocytic pathways [29, 30]. These alterations led to reduced endocytosis of recombinant enzymes used for replacement therapy, which was overcome by targeting the enzyme to an alternative route [29, 30]. To investigate whether similar alterations apply to other LSDs, here we have explored the endocytic behavior of NPC, Fabry, and Gaucher fibroblasts.

Clathrin-mediated endocytosis was the most affected pathway in all four diseases, in terms of both receptor-mediated (Tf) and fluid-phase transport. This agrees with previous observations in NPD and Pompe models of diminished clathrin-mediated uptake of ligands and cargo, including the mannose-6-phosphate receptor and recombinant therapeutic enzymes [28, 31]. Others have also reported deficits in synaptic neurotransmitter recycling, which depends on clathrin endocytosis [1], in mouse models of glucocerebrosidase deficiency (characteristic of Gaucher and Parkinson's disease) and palmitoyl protein thioesterase-1 deficiency (Batten disease) [26, 59]. This may contribute to the diminished synaptic plasticity, dopaminergenic neurotransmission, and other neurological symptoms observed in LSDs [6]. Diminished clathrin-mediated uptake may arise from decreased availability of endocytic machinery. Clathrin proteins, adapters, and other pathway constituents are directly involved

in the trafficking of lysosomal proteins in the biosynthetic route. For instance, mannose-6-phosphate receptors shuttle lysosomal enzymes between the trans-Golgi network and the lysosome in clathrin-coated vesicles [60]. Alteration of lysosomal content in LSDs may disturb the balance, display, and/or function of transmembrane and/or peripheral proteins involved in the signaling, coating, and fusion/fission events required for proper trafficking between these compartments [18, 53, 61]. This may lead to altered recycling and sequestration of said components at this stage, diminishing their availability to contribute to endocytic processes occurring at the plasmalemma. We recently reported increased localization of clathrin-heavy chain in perinuclear compartments and poor localization to ligand-receptor binding sites at the cell surface in NPD cells [30]. In view of this, a rigorous study examining the links between lysosomal dysfunction and the clathrin pathway is warranted.

In contrast, the relative activity of clathrin-independent pathways varied. NPD and NPC fibroblasts had the lowest levels of fluid-phase and receptor-mediated (CTB) uptake via caveolar endocytosis, whereas Gaucher and Fabry cells were less affected. Although the clathrin- and the caveolae-mediated pathways share some commonalities, e.g. use of dynamin and actin [1], there are also major differences between these pathways that may account for such distinction. For instance, the caveolar route is not directly involved in the biosynthetic or endocytic transport of lysosomal enzymes, and caveolar trafficking is known to bypass the lysosome in many cases in favor of Golgi and ER targets [62]. Therefore, this pathway may be less affected by lysosomal alterations. However, effects on this pathway may arise where lysosomal dysfunction alters the lipid composition of the plasmalemma or internal membranes. This is the case in this study, where the cholesterol and sphingomyelin levels in diseased cells directly related to the level of caveolar dysfunction. This agrees with previous studies showing aberrant trafficking of lactosylceramide and ganglioside ligands in these diseases (associated with caveolae), which were rerouted from a Golgi-targeting pathway to a lysosomal route [23, 24]. Others have also reported disruption of caveolar microdomains in a Batten disease model and poor recruitment of signaling molecules to lipid rafts in a Krabbe's disease model [25, 57].

With regard to macropinocytosis, the level of activity varied between diseases. The route was diminished in NPD cells, enhanced in NPC, and unchanged in Gaucher or Fabry cells. The relationship here with LSDs is less straightforward and may depend on collateral effects of the molecules and/or metabolic pathways affected. ASM activity is involved in macropinocytic-like events and is deficient in NPD, potentially explaining the deficits observed [29]. For instance, ASM increases the ceramide content of the plasmalemma, providing both the biophysical properties and actin reorganization required to sustain formation of large macropinocytic engulfment structures [63-67]. Since ASM is active in NPC, Gaucher and Fabry disease, this may explain the un-inhibited macropinocytosis in these cells. However, as NPC cells show defects in both clathrin- and caveolae-mediated pathways, it is possible that these cells upregulate macropinocytosis as a compensatory mechanism, as we observed here. Other cases of endocytic compensation have been reported elsewhere [68]. Since the caveolar route was still significantly active in Gaucher and Fabry cells, such compensation may not be necessary, rendering wild-type levels of macropinocytosis.

Endocytic disruption may arise directly from the primary genetic defect (such as the role of ASM in macropinocytosis) or secondarily to lysosomal stress (e.g. disruption of caveolar lipid rafts in NPD and NPC, or sequestration of clathrin machinery in the Golgi-lysosome route in all diseases tested). It is also possible that other physiochemical changes in the cell adversely affect endocytic function. For instance, the lysosomal buildup of undigested substances interferes with any pathways requiring lysosomal fusion/fission, pH, degradation, etc., such as autophagy, vesicular transport, and cytoskeletal reorganization [17, 19, 29, 30]. In fact, our results here showed reduced colocalization of internalized ligands of the clathrin and the caveolar pathways (Tf and CTB, respectively) with early endosomes and lysosomes. Others have also reported defects in other vesicular trafficking mechanisms, such as lysosomal exocytosis, which is required for plasmalemma recycling and proper display of membrane proteins, including endocytic receptors [61]. Interestingly, pharmacological enhancement of exocytosis is a concept that is being explored in order to enhance the therapeutic outcome of LSD treatments [53, 61, 69].

Differences with regard to the endocytic behavior of diseased cells are expected depending on the particular malady, specific mutations, and tissue type. Yet, the fact that cells of patients of four distinct diseases associated with different gene defects and lysosomal storages show endocytic alterations, which relates to previous reports in other LSD settings [19, 20, 22-31, 57], suggests a rather common pattern and validates our overall observations. Importantly, variations in uptake activity and endocytic trafficking in healthy vs. diseased cells represent important considerations for therapeutic delivery targeted to these routes. Clathrin activity is essential for replacement therapy for LSDs, as recombinant enzymes classically use this pathway for uptake (via the mannose-6-phosphate receptor) [21], and several other strategies have targeted other clathrin-dependent receptors [6, 70]. Targeting the caveolar route could help, but this pathway also appears affected in some diseases and material internalized via this pathway often avoids the lysosome [10, 34]. Strategies involving macropinocytosis may be possible by using certain signaling molecules (e.g. EGF), but because this is not a receptor-mediated pathway, cargo would remain dissolved in the fluid-phase, preventing specific or concentrated cargo from reaching the cell interior. Alternative, non-classical pathways may be beneficial, such as the case of the ICAM-1 example shown here [37, 38]. Interestingly, ICAM-1 mediates uptake via the CAM route, which requires ASM activity like macropinocytosis, yet it represents a receptor-mediated process that allows for specific targeting and concentration of cargo [37-39]. Also, coupling of recombinant ASM to ICAM-1 targeting carriers provides the necessary activity to recover this endocytic route [39, 71]. Enhanced lysosomal delivery via this route decreased storage and, subsequently, improved endocytosis.

Importantly, lipid (cholesterol) alterations in cellular membranes, arising from either the primary or secondary LSD defect, directly correlated with the degree of endocytic alteration. Although this may more directly and relevantly impact caveolar pathways due to the involvement of cholesterol, sphingolipids, etc. in this route, it is known that cholesterol and other lipids also play a role in clathrin-mediated uptake [72, 73]. Modulation of the levels of cholesterol, either directly with methyl-β-cyclodextrin, or indirectly with imipramine or recombinant ASM, permitted us to modify the overall endocytic activity, traced as bulk fluid-phase uptake. It is known that the lipid profile of membranes along the endo-lysosomal

pathway regulates the formation of lipid-protein complexes, the generation of membrane curvature, and the sorting of membrane-bound material [22, 74]. Lipids facing the compartment lumen, such as sphingolipids, regulate ion channel activity, affecting exocytosis and membrane remodeling [61]. Elevated cholesterol has been linked to aberrant SNARE protein complexes, disrupting compartment fusion en route to the lysosome [53]. Here, we only examined cells affected by primary lipid storage (NPD), but lipid storage also arises secondarily to carbohydrate and protein storage [61]. It would be worth performing similar studies on cells storing glycogen (Pompe disease), cysteine (cystinosis), autophagic materials (Huntington's, Alzheimer's, and Parkinson's disease), etc. [4, 16].

The relationship between storage and endocytic/trafficking dysfunction suggests that lysosomal toxicity arising from drugs and materials employed in drug delivery may render a similar phenotype. Lysosomal storage is a known side effect of many drugs used clinically, such as the case of imipramine (the anti-depressant used here), suramin (an anti-parasitic drug that diminishes proteolysis in Kupffer cells), chloroquine (a malariacidal agent), amiodarone (an antiarythmic), and certain anorectics [75]. Non-degradable drug carrier materials, such as quantum dots, gold, titanium dioxide, and others accumulate and impact lysosomal/autophagic compartments [76-80]. Intracellular delivery of lipids or slow-degradable polymers used in liposomes and other carrier formulations could render side effects consistent with lysosomal storage [80, 81]. Therefore, whether the cellular uptake and storage of foreign materials could alter endocytic function as observed in genetic LSDs deserves further investigation. Ultimately, awareness of the role of the lysosome in regulating endocytosis will improve therapeutic efficacy and diminish the toxicity of future drug delivery systems, including not only those aimed at treating LSDs, but also other diseases requiring endocytic entry within cells.

Supplementary Material

Refer to Web version on PubMed Central for supplementary material.

Acknowledgements

The authors thank Dr. Edward Schuchman (Dept. of Genetics and Genomic Sciences, Mount Sinai School of Medicine, New York, NY) for providing recombinant human ASM, as well as wild-type and NPD fibroblasts. This study was funded by NIH and NSF grants R01-HL098416 and CBET-1402756, respectively, to S. Muro. We also acknowledge a Howard Hughes Medical Institute fellowship to J. Rappaport under the University of Maryland Undergraduate Science Education Program; an NSF graduate research fellowship (DGE-0750616), University of Maryland Flagship fellowship, and NIH F31 fellowship (F31HL128121) to R. L. Manthe; and a fellowship from the Lysosomal Disease Network funded by a collaboration between NCATS and NIH (U54NS065768) to M. Solomon.

Abbreviations

ASM	acid sphingomyelinase
ICAM-1	intercellular adhesion molecule-1
LSD	lysosomal storage disease
NC	nanocarrier

NPD	type A-B Niemann-Pick disease
NPC	type C Niemann-Pick disease

References

1. Conner SD, Schmid SL. Regulated portals of entry into the cell. Nature. 2003; 422:37–44. [PubMed: 12621426]
2. Luzio JP, Pryor PR, Bright NA. Lysosomes: fusion and function. Nat. Rev. Mol. Cell Biol. 2007; 8:622–632. [PubMed: 17637737]
3. Duncan R, Richardson SC. Endocytosis and intracellular trafficking as gateways for nanomedicine delivery: opportunities and challenges. Mol. Pharm. 2012; 9:2380–2402. [PubMed: 22844998]
4. Manthe, RL.; Muro, S. Lysosomes and therapeutics: diseases, treatments, and side effects. In: Torchilin, V., editor. Handbook of Nanobiomedical Research. World Scientific Publishing Co.; Singapore: 2014. p. 261-305.
5. Rappaport, J.; Papademetriou, IT.; Muro, S. Endocytosis and the endolysosomal route in drug delivery. In: Muro, S., editor. Drug delivery across physiological barriers. Pan Stanford Ltd.; 2015. In press
6. Muro S. Strategies for delivery of therapeutics into the central nervous system for treatment of lysosomal storage disorders. Drug Deliv. and Trans. Res. 2012; 2:169–186.
7. Hillaireau H, Couvreur P. Nanocarriers' entry into the cell: relevance to drug delivery. Cell Mol. Life Sci. 2009; 66:2873–2896. [PubMed: 19499185]
8. Muro S. Challenges in design and characterization of ligand-targeted drug delivery systems. J. Control. Release. 2012; 164:125–137. [PubMed: 22709588]
9. McMahon HT, Boucrot E. Molecular mechanism and physiological functions of clathrin-mediated endocytosis. Nat. Rev. Mol. Cell Biol. 2011; 12:517–533. [PubMed: 21779028]
10. Bareford LM, Swaan PW. Endocytic mechanisms for targeted drug delivery. Adv. Drug Deliv. Rev. 2007; 59:748–758. [PubMed: 17659804]
11. Nichols B. Caveosomes and endocytosis of lipid rafts. J. Cell Sci. 2003; 116:4707–4714. [PubMed: 14600257]
12. McIntosh DP, Tan XY, Oh P, Schnitzer JE. Targeting endothelium and its dynamic caveolae for tissue-specific transcytosis in vivo: a pathway to overcome cell barriers to drug and gene delivery. Proc. Natl. Acad. Sci. U S A. 2002; 99:1996–2001. [PubMed: 11854497]
13. Gong Q, Huntsman C, Ma D. Clathrin-independent internalization and recycling. J. Cell. Mol. Med. 2008; 12:126–144. [PubMed: 18039352]
14. Stan RV. Endocytosis pathways in endothelium: how many? Am. J. Physiol. Lung Cell. Mol. Physiol. 2006; 290:L806–L808. [PubMed: 16603594]
15. Serrano, D.; Muro, S. Endothelial cell adhesion molecules in drug delivery applications. In: Aranda-Espinoza, H., editor. Mechanobiology of the endothelium. CRC Press; Boca Raton: 2014. p. 185-226.
16. Futerman AH, van Meer G. The cell biology of lysosomal storage disorders. Nat. Rev. Mol. Cell Biol. 2004; 5:554–565. [PubMed: 15232573]
17. Parkinson-Lawrence EJ, Shandala T, Prodoehl M, Plew R, Borlace GN, Brooks DA. Lysosomal storage disease: revealing lysosomal function and physiology. Physiology (Bethesda). 2010; 25:102–115. [PubMed: 20430954]
18. Ballabio A, Gieselmann V. Lysosomal disorders: from storage to cellular damage. Biochim. Biophys. Acta. 2009; 1793:684–696. [PubMed: 19111581]
19. Fukuda T, Ewan L, Bauer M, Mattaliano RJ, Zaal K, Ralston E, Plotz PH, Raben N. Dysfunction of endocytic and autophagic pathways in a lysosomal storage disease. Ann. Neurol. 2006; 59:700–708. [PubMed: 16532490]
20. Simons K, Gruenberg J. Jamming the endosomal system: lipid rafts and lysosomal storage diseases. Trends Cell Biol. 2000; 10:459–462. [PubMed: 11050411]

21. Desnick RJ, Schuchman EH. Enzyme replacement and enhancement therapies: lessons from lysosomal disorders. Nat. Rev. Genet. 2002; 3:954–966. [PubMed: 12459725]
22. Marks DL, Pagano RE. Endocytosis and sorting of glycosphingolipids in sphingolipid storage disease. Trends Cell Biol. 2002; 12:605–613. [PubMed: 12495850]
23. Puri V, Watanabe R, Singh RD, Dominguez M, Brown JC, Wheatley CL, Marks DL, Pagano RE. Clathrin-dependent and -independent internalization of plasma membrane sphingolipids initiates two Golgi targeting pathways. J. Cell Biol. 2001; 154:535–547. [PubMed: 11481344]
24. Hortsch R, Lee E, Erathodiyil N, Hebbar S, Steinert S, Lee JY, Chua DS, Kraut R. Glycolipid trafficking in Drosophila undergoes pathway switching in response to aberrant cholesterol levels. Mol. Biol. Cell. 2010; 21:778–790. [PubMed: 20053687]
25. Tecedor L, Stein CS, Schultz ML, Farwanah H, Sandhoff K, Davidson BL. CLN3 loss disturbs membrane microdomain properties and protein transport in brain endothelial cells. J. Neurosci. 2013; 33:18065–18079. [PubMed: 24227717]
26. Aby E, Gumps K, Roth A, Sigmon S, Jenkins SE, Kim JJ, Kramer NJ, Parfitt KD, Korey CA. Mutations in palmitoyl-protein thioesterase 1 alter exocytosis and endocytosis at synapses in Drosophila larvae. Fly (Austin). 2013; 7:267–279. [PubMed: 24091420]
27. Liscum L, Faust JR. Low density lipoprotein (LDL)-mediated suppression of cholesterol synthesis and LDL uptake is defective in Niemann-Pick type C fibroblasts. J. Biol. Chem. 1987; 262:17002–17008. [PubMed: 3680287]
28. Dhami R, Schuchman EH. Mannose 6-phosphate receptor-mediated uptake is defective in acid sphingomyelinase-deficient macrophages: implications for Niemann-Pick disease enzyme replacement therapy. J. Biol. Chem. 2004; 279:1526–1532. [PubMed: 14557264]
29. Rappaport J, Manthe RL, Garnacho C, Muro S. Altered clathrin-independent endocytosis in type A Niemann-Pick disease cells and rescue by ICAM-1-targeted enzyme delivery. Mol. Pharm. 2015; 12:1366–1376. [PubMed: 25849869]
30. Rappaport J, Garnacho C, Muro S. Clathrin-mediated endocytosis is impaired in type A-B Niemann-Pick disease model cells and can be restored by ICAM-1-mediated enzyme replacement. Mol. Pharm. 2014; 11:2887–2895. [PubMed: 24949999]
31. Cardone M, Porto C, Tarallo A, Vicinanza M, Rossi B, Polishchuk E, Donaudy F, Andria G, De Matteis MA, Parenti G. Abnormal mannose-6-phosphate receptor trafficking impairs recombinant alpha-glucosidase uptake in Pompe disease fibroblasts. Pathogenetics. 2008; 1:6–28. [PubMed: 19046416]
32. Patterson, MC.; Vanier, MT.; Suzuki, K.; Morris, JA.; Carstea, E.; Neufeld, EB.; Blanchette-Mackie, JE.; Pentchev, PG. Niemann-Pick Disease Type C: A lipid trafficking disorder. In: Valle, D.; Beaudet, AL.; Vogelstein, B.; Kinzler, KW.; Antonarakis, SE.; Ballabio, A.; Gibson, K.; Mitchell, G., editors. The Online Metabolic and Molecular Bases of Inherited Disease. McGraw-Hill; New York: 2014. Chapter 145
33. Desnick, RJ.; Ioannou, YA.; Eng, CM. α-Galactosidase A deficiency: Fabry disease. In: Valle, D.; Beaudet, AL.; Vogelstein, B.; Kinzler, KW.; Antonarakis, SE.; Ballabio, A.; Gibson, K.; Mitchell, G., editors. The Online Metabolic and Molecular Bases of Inherited Disease. McGraw-Hill; New York: 2014. Chapter 150
34. Grabowski, GA.; Petsko, GA.; Kolodny, EH. Gaucher Disease. In: Valle, D.; Beaudet, AL.; Vogelstein, B.; Kinzler, KW.; Antonarakis, SE.; Ballabio, A.; Gibson, K.; Mitchell, G., editors. The Online Metabolic and Molecular Bases of Inherited Disease. McGraw-Hill; New York: 2014. Chapter 146
35. He X, Miranda SR, Xiong X, Dagan A, Gatt S, Schuchman EH. Characterization of human acid sphingomyelinase purified from the media of overexpressing Chinese hamster ovary cells. Biochim. Biophys. Acta. 1999; 1432:251–264. [PubMed: 10407147]
36. Muro, S. Intercellular adhesion molecule-1 and vascular cell adhesion molecule-1. In: Aird, W., editor. Endothelial Biomedicine. Cambridge University Press; New York: 2007. p. 1058-1070.
37. Muro S, Wiewrodt R, Thomas A, Koniaris L, Albelda SM, Muzykantov VR, Koval M. A novel endocytic pathway induced by clustering endothelial ICAM-1 or PECAM-1. J. Cell Sci. 2003; 116:1599–1609. [PubMed: 12640043]

38. Muro S, Schuchman EH, Muzykantov VR. Lysosomal enzyme delivery by ICAM-1-targeted nanocarriers bypassing glycosylation- and clathrin-dependent endocytosis. Mol. Ther. 2006; 13:135–141. [PubMed: 16153895]
39. Serrano D, Bhowmick T, Chadha R, Garnacho C, Muro S. ICAM-1 engagement modulates sphingomyelinase and ceramide, supporting uptake of drug carriers by the vascular endothelium. Arterioscler. Thromb. Vasc. Biol. 2012; 32:1178–1185. [PubMed: 22328778]
40. Hsu J, Northrup L, Bhowmick T, Muro S. Enhanced delivery of α-glucosidase for Pompe disease by ICAM-1-targeted nanocarriers: comparative performance of a strategy for three distinct lysosomal storage disorders. Nanomedicine. 2012; 8:731–739. [PubMed: 21906578]
41. Hsu J, Serrano D, Bhowmick T, Kumar K, Shen Y, Kuo YC, Garnacho C, Muro S. Enhanced endothelial delivery and biochemical effects of α-galactosidase by ICAM-1-targeted nanocarriers for Fabry disease. J. Control. Release. 2011; 149:323–331. [PubMed: 21047542]
42. Muro S, Dziubla T, Qiu W, Leferovich J, Cui X, Berk E, Muzykantov VR. Endothelial targeting of high-affinity multivalent polymer nanocarriers directed to intercellular adhesion molecule 1. J. Pharmacol. Exp. Ther. 2006; 317:1161–1169. [PubMed: 16505161]
43. Garnacho C, Dhami R, Simone E, Dziubla T, Leferovich J, Schuchman EH, Muzykantov V, Muro S. Delivery of acid sphingomyelinase in normal and Niemann-Pick disease mice using intercellular adhesion molecule-1-targeted polymer nanocarriers. J. Pharmacol. Exp. Ther. 2008; 325:400–408. [PubMed: 18287213]
44. Hurwitz R, Ferlinz K, Sandhoff K. The tricyclic antidepressant desipramine causes proteolytic degradation of lysosomal sphingomyelinase in human fibroblasts. Biol. Chem. Hoppe Seyler. 1994; 375:447–450. [PubMed: 7945993]
45. Liu B. Therapeutic potential of cyclodextrins in the treatment of Niemann–Pick type C disease. Clin. Lipidol. 2012; 7:289–301. [PubMed: 25152773]
46. Kirkham M, Parton RG. Clathrin-independent endocytosis: new insights into caveolae and non-caveolar lipid raft carriers. Biochim. Biophys. Acta. 2005; 1745:273–286. [PubMed: 16046009]
47. Torgersen ML, Skretting G, van Deurs B, Sandvig K. Internalization of cholera toxin by different endocytic mechanisms. J. Cell Sci. 2001; 114(Pt 20):3737–3747. [PubMed: 11707525]
48. Damke H, Baba T, van der Bliek AM, Schmid SL. Clathrin-independent pinocytosis is induced in cells overexpressing a temperature-sensitive mutant of dynamin. J Cell Biol. 1995; 131:69–80. [PubMed: 7559787]
49. Mayor S, Pagano RE. Pathways of clathrin-independent endocytosis. Nat. Rev. Mol. Cell Biol. 2007; 8:603–612. [PubMed: 17609668]
50. Singh RD, Puri V, Valiyaveettil JT, Marks DL, Bittman R, Pagano RE. Selective caveolin-1-dependent endocytosis of glycosphingolipids. Mol. Biol. Cell. 2003; 14:3254–3265. [PubMed: 12925761]
51. Zhang Y, Zhang L, Li Y, Sun S, Tan H. Different contributions of clathrin- and caveolae-mediated endocytosis of vascular endothelial cadherin to lipopolysaccaride-induced vascular hyperpermeability. PLoS ONE. 2014; 9:e106328. [PubMed: 25180771]
52. Stan RV. Structure and function of endothelial caveolae. Microsc. Res. Tech. 2002; 57:350–364. [PubMed: 12112442]
53. Fraldi A, Annunziata F, Lombardi A, Kaiser HJ, Medina DL, Spampanato C, Fedele AO, Polishchuk R, Sorrentino NC, Simons K, Ballabio A. Lysosomal fusion and SNARE function are impaired by cholesterol accumulation in lysosomal storage disorders. Embo j. 2010; 29:3607–3620. [PubMed: 20871593]
54. Puri V, Watanabe R, Dominguez M, Sun X, Wheatley CL, Marks DL, Pagano RE. Cholesterol modulates membrane traffic along the endocytic pathway in sphingolipid-storage diseases. Nat. Cell Biol. 1999; 1:386–388. [PubMed: 10559968]
55. Calderon AJ, Muzykantov V, Muro S, Eckmann DM. Flow dynamics, binding and detachment of spherical carriers targeted to ICAM-1 on endothelial cells. Biorheology. 2009; 46:323–341. [PubMed: 19721193]
56. Bhowmick T, Berk E, Cui X, Muzykantov VR, Muro S. Effect of flow on endothelial endocytosis of nanocarriers targeted to ICAM-1. J. Control. Release. 2012; 157:485–492. [PubMed: 21951807]

57. Teixeira CA, Miranda CO, Sousa VF, Santos TE, Malheiro AR, Solomon M, Maegawa GH, Brites P, Sousa MM. Early axonal loss accompanied by impaired endocytosis, abnormal axonal transport, and decreased microtubule stability occur in the model of Krabbe's disease. Neurobiology of disease. 2014; 66:92–103. [PubMed: 24607884]
58. Schuchman, E.; Desnick, R. Niemann-Pick disease types A and B: acid sphingomyelinase deficiencies. In: Scriver, C.; Beaudet, A.; Sly, W.; Valle, D.; Childs, B.; Kinzler, K.; Vogelstein, B., editors. The Metabolic and Molecular Bases of Inherited Disease. McGraw-Hill; New York: 2000. p. 3589-3610.
59. Ginns EI, Mak SK, Ko N, Karlgren J, Akbarian S, Chou VP, Guo Y, Lim A, Samuelsson S, LaMarca ML, Vazquez-DeRose J, Manning-Bog AB. Neuroinflammation and alpha-synuclein accumulation in response to glucocerebrosidase deficiency are accompanied by synaptic dysfunction. Mol. Genet. Metab. 2014; 111:152–162. [PubMed: 24388731]
60. Braulke T, Bonifacino JS. Sorting of lysosomal proteins. Biochim. Biophys. Acta. 2009; 1793:605–614. [PubMed: 19046998]
61. Samie MA, Xu H. Lysosomal exocytosis and lipid storage disorders. J. Lipid Res. 2014; 55:995–1009. [PubMed: 24668941]
62. Pelkmans L. Secrets of caveolae- and lipid raft-mediated endocytosis revealed by mammalian viruses. Biochim. Biophys. Acta. 2005; 1746:295–304. [PubMed: 16126288]
63. Fernandes MC, Cortez M, Flannery AR, Tam C, Mortara RA, Andrews NW. Trypanosoma cruzi subverts the sphingomyelinase-mediated plasma membrane repair pathway for cell invasion. J. Exp. Med. 2011; 208:909–921. [PubMed: 21536739]
64. Zeidan YH, Jenkins RW, Hannun YA. Remodeling of cellular cytoskeleton by the acid sphingomyelinase/ceramide pathway. J. Cell Biol. 2008; 181:335–350. [PubMed: 18426979]
65. Falkow S, Isberg RR, Portnoy DA. The interaction of bacteria with mammalian cells. Annu. Rev. Cell Biol. 1992; 8:333–363. [PubMed: 1476803]
66. Miller ME, Adhikary S, Kolokoltsov AA, Davey RA. Ebolavirus requires acid sphingomyelinase activity and plasma membrane sphingomyelin for infection. J. Virol. 2012; 86:7473–7483. [PubMed: 22573858]
67. Grassme H, Becker KA, Zhang Y, Gulbins E. Ceramide in bacterial infections and cystic fibrosis. Biol. Chem. 2008; 389:1371–1379. [PubMed: 18783339]
68. Doherty GJ, McMahon HT. Mechanisms of endocytosis. Annu. Rev. Biochem. 2009; 78:857–902. [PubMed: 19317650]
69. Xu M, Liu K, Swaroop M, Porter FD, Sidhu R, Firnkes S, Ory DS, Marugan JJ, Xiao J, Southall N, Pavan WJ, Davidson C, Walkley SU, Remaley AT, Baxa U, Sun W, McKew JC, Austin CP, Zheng W. γ-tocopherol reduces lipid accumulation in Niemann-Pick type C1 and Wolman cholesterol storage disorders. J. Biol. Chem. 2012; 287:39349–39360. [PubMed: 23035117]
70. Qian ZM, Li H, Sun H, Ho K. Targeted drug delivery via the transferrin receptor-mediated endocytosis pathway. Pharmacol. Rev. 2002; 54:561–587. [PubMed: 12429868]
71. Ansar M, Serrano D, Papademetriou I, Bhowmick TK, Muro S. Biological functionalization of drug delivery carriers to bypass size restrictions of receptor-mediated endocytosis independently from receptor targeting. ACS Nano. 2013; 7:10597–10611. [PubMed: 24237309]
72. Kozik P, Hodson NA, Sahlender DA, Simecek N, Soromani C, Wu J, Collinson LM, Robinson MS. A human genome-wide screen for regulators of clathrin-coated vesicle formation reveals an unexpected role for the V-ATPase. Nat. Cell Biol. 2013; 15:50–60. [PubMed: 23263279]
73. Rodal SK, Skretting G, Garred O, Vilhardt F, van Deurs B, Sandvig K. Extraction of cholesterol with methyl-beta-cyclodextrin perturbs formation of clathrin-coated endocytic vesicles. Mol. Biol. Cell. 1999; 10:961–974. [PubMed: 10198050]
74. Choudhury A, Sharma DK, Marks DL, Pagano RE. Elevated endosomal cholesterol levels in Niemann-Pick cells inhibit rab4 and perturb membrane recycling. Mol. Biol. Cell. 2004; 15:4500–4511. [PubMed: 15292453]
75. Schneider P, Korolenko TA, Busch U. A review of drug-induced lysosomal disorders of the liver in man and laboratory animals. Microsc. Res. Tech. 1997; 36:253–275. [PubMed: 9140926]
76. Li R, Ji Z, Qin H, Kang X, Sun B, Wang M, Chang CH, Wang X, Zhang H, Zou H, Nel AE, Xia T. Interference in autophagosome fusion by rare earth nanoparticles disrupts autophagic flux and

regulation of an interleukin-1beta producing inflammasome. ACS Nano. 2014; 8:10280–10292. [PubMed: 25251502]

77. Ding F, Li Y, Liu J, Liu L, Yu W, Wang Z, Ni H, Liu B, Chen P. Overendocytosis of gold nanoparticles increases autophagy and apoptosis in hypoxic human renal proximal tubular cells. Int. J. Nanomedicine. 2014; 9:4317–4330. [PubMed: 25246788]
78. Stern ST, Adiseshaiah PP, Crist RM. Autophagy and lysosomal dysfunction as emerging mechanisms of nanomaterial toxicity. Part. Fibre Toxicol. 2012; 9:20–35. [PubMed: 22697169]
79. Stearns RC, Paulauskis JD, Godleski JJ. Endocytosis of ultrafine particles by A549 cells. Am. J .Respir. Cell Mol. Biol. 2001; 24:108–115. [PubMed: 11159043]
80. Frohlich E. Cellular targets and mechanisms in the cytotoxic action of non-biodegradable engineered nanoparticles. Curr. Drug Metab. 2013; 14:976–988. [PubMed: 24160294]
81. Song W, Soo Lee S, Savini M, Popp L, Colvin VL, Segatori L. Ceria nanoparticles stabilized by organic surface coatings activate the lysosome-autophagy system and enhance autophagic clearance. ACS Nano. 2014; 8:10328–10342. [PubMed: 25315655]

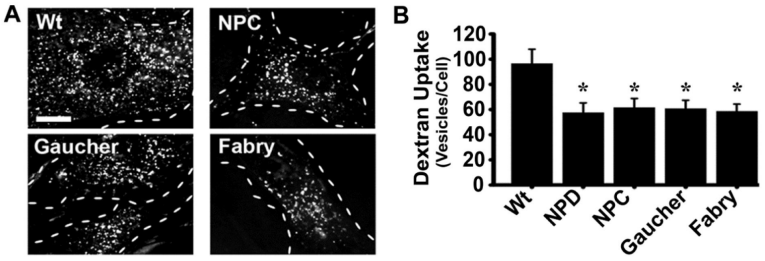

Figure 1.

Bulk pinocytic fluid-phase uptake in LSD fibroblasts. (A) Fluorescence microscopy images of wild-type (Wt), NPC, Gaucher, and Fabry fibroblasts incubated for 1 h at 37°C with cell medium containing Texas Red dextran. NPD, reported in [30], serves as a control and is not shown. Dashed lines = cell borders, as observed by phase-contrast microscopy. Scale bar = 10 μm. (B) Quantification of the number of dextran-positive vesicles. Data are the mean ± SEM. *Comparison with Wt ($p<0.05$ by Student's t-test).

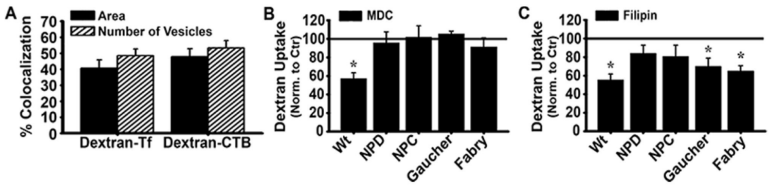

Figure 2.

Fluid-phase uptake via clathrin- or caveolae-mediated endocytosis in LSD fibroblasts. (A) Quantification of the percent colocalization of Texas Red dextran-positive vesicles internalized by wild-type fibroblasts (30 min, 37°C) along with green fluorescent transferrin (Tf) or cholera toxin B (CTB). Colocalizing area and number of vesicles are shown. (B, C) Quantification of the number of Texas Red dextran-positive vesicles internalized during 1 h at 37°C by wild-type vs. diseased cells incubated with: (B) monodansylcadaverine (MDC), an inhibitor of clathrin-mediated endocytosis, or (C) filipin, an inhibitor of caveolar endocytosis. Data are normalized to those of cells incubated in the absence of inhibitors (control (Ctr)), which is indicated by the horizontal line. The difference between the control line and the inhibitor bar demonstrates the relative contribution of each pathway to fluid-phase uptake. Data are the mean ± SEM. *Comparison with uninhibited, control cells ($p<0.05$ by Student's t-test).

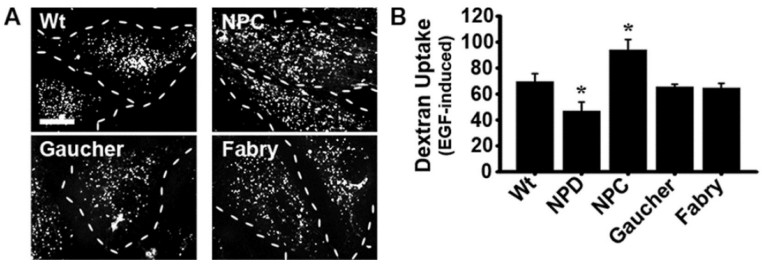

Figure 3.

Fluid-phase uptake via macropinocytosis in LSD fibroblasts. Incubation of Wt, NPD, NPC, Gaucher, and Fabry fibroblasts for 1 h at 37°C with cell medium containing both the fluid-phase marker Texas Red dextran and epidermal growth factor (EGF), which stimulates macropinocytosis. (A) Fluorescence images showing dextran-positive vesicles. NPD, reported in [29] serves as a control and is not shown. Dashed lines = cell borders, as observed by phase-contrast microscopy. Scale bar = 10 μm. (B) Quantification of the number of dextran-positive vesicles. Data are the mean ± SEM. *Comparison with Wt ($p<0.05$ by Student's t-test).

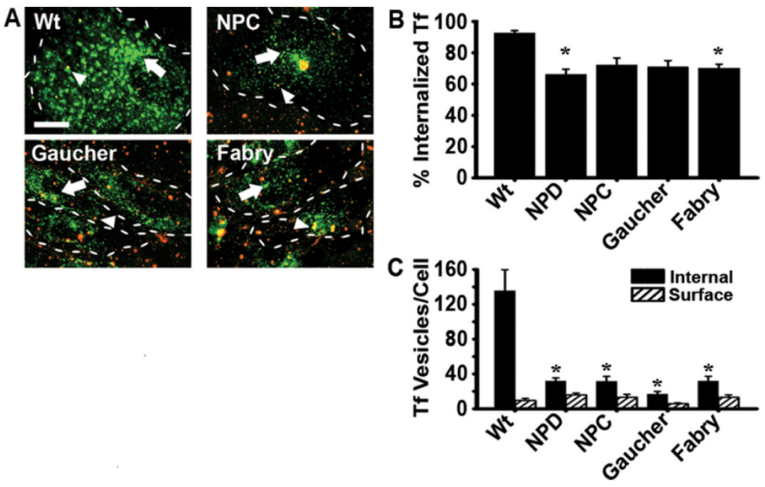

Figure 4.

Transferrin endocytosis in LSD fibroblasts. Wild-type (Wt), NPD, NPC, Gaucher, and Fabry fibroblasts incubated with fluorescent transferrin (Tf; green pseudocolor) for 1 h at 37°C. (A) Fluorescence images were taken after unbound Tf was washed off and surface-bound Tf was immunostained (red pseudocolor). This rendered surface-bound Tf marked in two colors (red + green = yellow; arrowheads), distinguishable from internalized Tf (green; arrows). NPD, reported in [30] serves as a control and is not shown. Dashed lines = cell borders, as observed from phase-contrast microscopy. Scale bar = 10 μm. (B) Quantification of the percentage of single-labeled Tf found inside each cell compared to total (single-labeled and double-labeled) Tf associated with said cells. (C) Internal and surface Tf (fluorescent objects over background). (B,C) Data are the mean ± SEM. *Comparison with Wt ($p<0.05$ by Student's t-test).

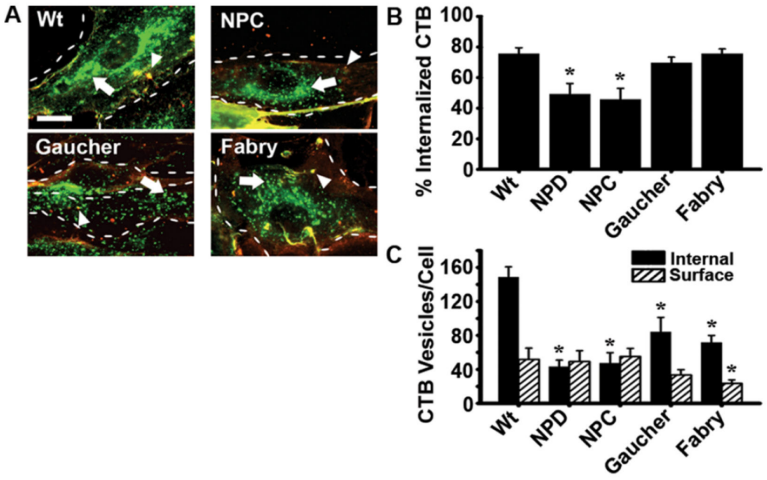

Figure 5.

Internalization of cholera toxin B in LSD fibroblasts. Wild-type (Wt), NPD, NPC, Gaucher, and Fabry fibroblasts incubated with fluorescent cholera toxin B (CTB; green pseudocolor) for 1 h at 37°C. (A) Fluorescence images were taken after unbound CTB was washed off and surface-bound CTB was immunostained (red pseudocolor). This rendered surface-bound CTB marked in two colors (red + green = yellow; arrowheads), distinguishable from internalized CTB (green; arrows). NPD, reported in [29] serves as a control and is not shown. Dashed lines = cell borders, as observed from phase-contrast microscopy. Scale bar = 10 μm. (B) Quantification of the percentage of single-labeled CTB found inside each cell compared to total CTB (single-labeled and double-labeled) associated with said cells. (C) Internal and surface CTB (fluorescent objects over background). (B,C) Data are the mean ± SEM. *Comparison with Wt ($p<0.05$ by Student's t-test).

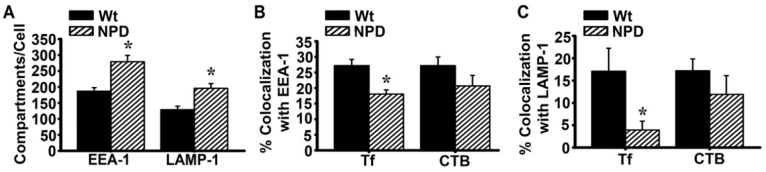

Figure 6.

Intracellular trafficking of ligands in LSD fibroblasts. Wild-type (Wt) or NPD fibroblasts were incubated for 30 min at 37°C with fluorescent transferrin (Tf) or cholera toxin B (CTB), pseudocolored green, followed by immunostaining of early endosomes or lysosomes using antibodies against EEA-1 or LAMP-1, respectively (pseudocolored red). (A) The graph shows the quantification of the number of EEA-1- or anti-LAMP-1-positive vesicles from fluorescence microscopy images (Suppl. Fig. 5). (B) Colocalization of Tf or CTB with EEA-1, and (C) with LAMP-1, expressed as the percentage of the total Tf or CTB associated to cells. Data are the mean ± SEM. *Comparison with wild-type cells ($p<0.05$ by Student's t-test).

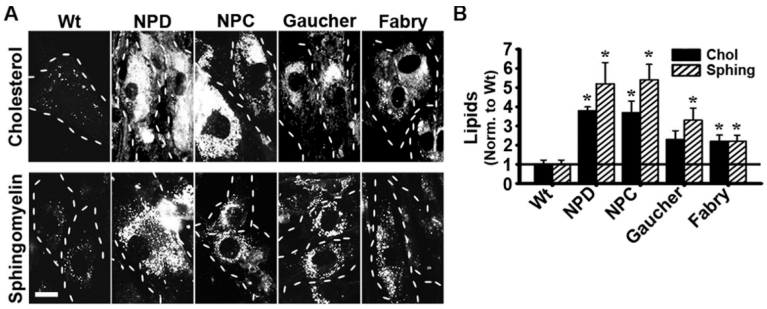

Figure 7.

Lipid accumulation in LSD fibroblasts. (A) Fluorescence images of wild-type (Wt), NPD, NPC, Gaucher, and Fabry fibroblasts incubated overnight with fluorescent BODIPY-FL-C_{12}-sphingomyelin or stained with filipin, in order to visualize sphingomyelin and cholesterol, respectively. Dashed lines = cell borders, as observed from phase-contrast microscopy. Scale bar = 10 μm. (B) Quantification of lipid accumulation, normalized to that of Wt cells (horizontal bar). Data are the mean ± SEM. *Comparison with Wt ($p<0.05$ by Student's t-test).

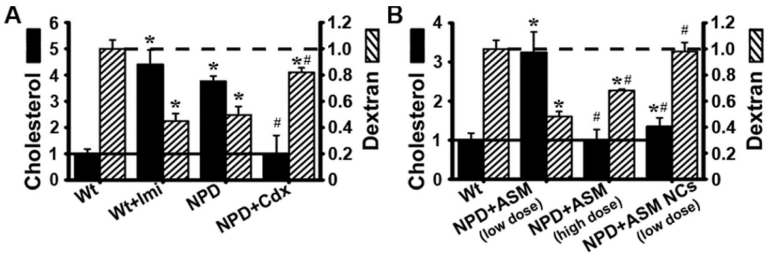

Figure 8.

Cholesterol levels are inversely proportional to bulk endocytosis in NPD fibroblasts. (A) Wild-type (Wt) fibroblasts were treated at 37°C for 48 h with imipramine (imi) to induce lipid storage and NPD fibroblasts were treated for 1 h at 37°C with methyl-β -cyclodextrin (Cdx) to relieve lipid storage. (B) NPD fibroblasts were treated for 1 h at 37°C with cell medium containing naked ASM (low dose = 32 nM; high dose = 320 nM) or nanocarriers targeted to ICAM-1 and containing 32 nM ASM (anti-ICAM/ASM NCs). (A, B) After 1 h incubation with Cdx or enzyme, these agents were removed and cells incubated for an additional 2 h in control medium. Cholesterol levels were quantified using fluorescent filipin staining and normalized to that of Wt cells. The number of Texas Red dextran-positive vesicles internalized within cells after 1 h incubation at 37°C was quantified by fluorescence microscopy, as in Fig. 1. Data are the mean ± SEM. *Comparison with untreated Wt (solid horizontal line in graphs). #Comparison with untreated NPD (dashed horizontal line in graphs) ($p<0.05$ by Student's t-test).